Composite Structures 165 (2016) 266–272

Contents lists available at ScienceDirect

Composite Structures

journal homepage: www.elsevier.com/locate/compstruct

Dynamic compressive response of wrapped carbon fibre composite corrugated cores

Tao Liu *, Paul Turner

Centre for Structural Engineering and Informatics, Composites Research Group, Department of Civil Engineering, University of Nottingham, University Park, Nottingham NG7 2RD, UK
Faculty of Engineering, University of Nottingham, University Park, Nottingham NG7 2RD, UK

ARTICLE INFO

Article history:
Received 18 May 2016
Revised 17 October 2016
Accepted 19 October 2016
Available online 20 October 2016

Keywords:
Composite sandwich structures
High strain rate
Strain rate sensitivity
Dynamic compression

ABSTRACT

The experimental study on the compressive response of the carbon fibre composite sandwich structures with corrugated cores is reported. The corrugated core was manufactured from unidirectional carbon fibre pre-impregnated lamina wrapped around destructible triangular prisms. Individual wrapped triangular composite cores of relative density $\bar{\rho} \approx 0.13$ are cut from the sandwich beams and tested under both quasi-static compression and dynamic compression at a strain rate up to 8200 s^{-1} using an instrumented direct impact Kolsky bar experiment. Under quasi-static compressive test, as the cores were provided with no lateral confinement, the failure mechanism of the composite core was that of progressive unwrapping of cores due to matrix cracking at the joints of the core webs. Under the dynamic compressive tests, the composite cores demonstrated rate-dependent behaviour. The strain rate dependency was attributed to the suppression of the quasi-static "unwrapping" failure mechanism, and inertial stabilisation of the struts against buckling leading to an upper-bound failure mechanism of crushing of carbon fibre material within the struts.

1. Introduction

Lightweight sandwich structures can offer greater structural performance than their monolithic counterparts under certain loading scenarios, e.g. their high bending strength to weight ratio can yield great weight-saving benefits for structural elements under bending and shear [1]. There has been an increasing interest in the application of sandwich structures for impact protection or blast mitigation [2,3]. Compared to a monolithic panel of equal areal mass, sandwich panels can offer a two-fold approach for increasing resistance to frontal shock loading, i.e. (i) increased flexural strength and (ii) a reduction of the transmitted shock impulse into the structure via the fluid-structure interaction (FSI) effects [4]. The effect of fluid-structure interaction is significant for water blast but relatively unimportant for air blast.

Development of high performance blast resistant sandwich structures has been mainly based on two types of sandwich core topologies, i.e. foam cores and periodic cellular cores. Inexpensive metallic or polymeric foams with stochastic closed cells are relatively easy for manufacturing [5,6] and prove to be excellent at absorbing energy during impact events [5]. However, their stochastic nature leads to curves and undulations within the cell walls, reducing their compressive properties [7]. It has been demonstrated that the deformation mode of the microstructure of stochastic foams is "bending-dominated" under macroscopic stresses [8,9]. This leads to the stiffness and strength scaling with $\bar{\rho}^2$ and $\bar{\rho}^{1.5}$, respectively, with $\bar{\rho}$ as the relative density of the foams [5]. Periodic cellular cores include those with two dimensional (2D) microstructures, such as honeycombs and corrugated cores as well as those with three dimensional (3D) microstructures, such as truss lattices. Truss lattices can be arranged with a tetrahedral, pyramidal or Kagome topology at the length scale of 0.5 to 15 mm. They can offer superior peak strengths at low relative densities [10,11]. They have been shown to exhibit 'stretch-dominated' deformation mechanism that provides about 10 times enhanced stiffness when compared with that of stochastic foams [12]. With less complexity in manufacturing compared to truss lattices, honeycombs and corrugated cores can offer good performance for blast protection owing to high compressive and transverse shear strengths [4,13].

Existing research have mainly focused on metallic sandwich structures [14], and have recently moved to composite sandwich structures, e.g. E-glass composite corrugated cores by Russell et al. [15] using stitching technique, and carbon fibre epoxy square

* Corresponding author at: Centre for Structural Engineering and Informatics, Composites Research Group, Department of Civil Engineering, University of Nottingham, University Park, Nottingham NG7 2RD, UK.
E-mail address: Tao.Liu@nottingham.ac.uk (T. Liu).

http://dx.doi.org/10.1016/j.compstruct.2016.10.080
0263-8223/

honeycomb cores by Russell et al. [16] using slotted composite sheet methodology. The inherent high stiffness and strength and low density of fibre reinforced composite materials mean that they are ideally suited for use in lightweight sandwich panel design. Recent investigation has demonstrated the scenarios that fibre reinforced composite structures can outperform metallic structures under shock loadings [17]. However, due to their brittle nature and relatively complicated manufacturing processes, the design of an efficient composite structural sandwich panel system can prove difficult. This paper presents a novel solution using wrapped composite corrugated cores of low relative density for potential use of protection against dynamic compressive loading. In Section 2, it begins with a description of the material and the manufacturing technique employed for the creation of laboratory scale wrapped carbon-fibre composite cores. In Section 3, the experimental protocols for both quasi-static tests and dynamic compressive test are described. The quasi-static responses of the constitutive composite material and the wrapped cores are presented. In Section 4, the dynamic compressive responses of both the constitutive composite material and the wrapped cores are investigated utilising a direct impact Kolsky bar experiment.

2. Materials and manufacturing

Wrapped composite sandwich cores were manufactured using MTM57-T700 unidirectional carbon fibre/epoxy resin Pre-preg supplied by Cytec Solvay Group. The Pre-preg was made of Toray T700 fibre with diameter 7 μm and toughened epoxy resin with 35% fibre fraction by weight. Each layer of the composite material had a thickness of approximately 0.70 mm, a density $\rho_c = 1.22\ \mathrm{g/cm^3}$ and a Poisson's ratio $v = 0.3$ after cure.

The manufacturing process of the sandwich plate is schematically shown in Fig. 1. Powder based, destructible triangular prisms of base width $\lambda = 30$ mm and height $h = 15$ mm, acting as the internal mould, were manufactured using a rapid prototyping (RP) technique. The prisms were wrapped with PET based release tapes to allow for ease of demoulding post curing. Single layered pre-impregnated laminate tapes were then wrapped around each prism with an approximate overlap of each layer of 15 mm, located at the base of the isosceles triangle (Fig. 1(b)). The wrapped moulds were then arranged edge to edge, shown in Fig. 1(c), to create a full sandwich cores. Standard vacuum bagging technique was then employed for composite curing at atmospheric pressure. A Quicklock Thermoclave autoclave heated the plate for 3 h at 120 °C to facilitate curing (Fig. 1(d)). UD-laminate facesheets were then adhered to the top and bottom surfaces of the cores using Loctite Hysol© 9461 A&B epoxy adhesive of 1:1 mixture ratio. The facesheets consisted of 4 stacked plies in $[0/90]_2$ configuration giving a total thickness of 2.8 mm. The sandwich plate was clamped with a constant pressure at room temperature for 3 days to acquire full adhesive strength for the interfaces between the facesheets and the corrugated core (Fig. 1(e)). The fibre orientation of both the corrugated core webs and facesheets is shown in Fig. 1(e) under local 1-2-3 coordinate systems with 1-axis aligned with fibre direction. A sandwich beam after completion is shown in Fig. 1(f). The geometry of a representative unit cell of the corrugated core sandwich plate after cure is shown in Fig. 2 under the global x-y-z coordinate system, with base length $L = 30$ mm and height $h = 15$ mm, core web thickness $t_c = 1.4$ mm. The relative density of the corrugated core, defined as the ratio of the core density and the base material density, is 0.13. In compressive testing described next, individual corrugated core specimen were cut from the sandwich plate.

3. Experimental protocols

3.1. Tensile coupon test on the base material

Quasi-static (2 mm/min) uniaxial tension material coupon tests were conducted on the base composite material in order to determine the in-plane mechanical properties. A screw-driven Instron© 5581 type testing machine with a static 50kN load cell was utilised for testing. For tensile tests, dog bone shaped samples were employed following EN ISO 527-4 test method. The dog bone samples had width of 10 mm and a gauge length of 50 mm. The axial nominal strain was measured using an Instron 2630 series clip-on extensometer and confirmed using a single Stingray© F-146B Firewire Camera video gauge with post processing software Imetrum Video Gauge©. The load was measured directly from the test machine crosshead. The clip-on extensometer was removed prior to failure of the sample. Samples were tested with fibres orientated

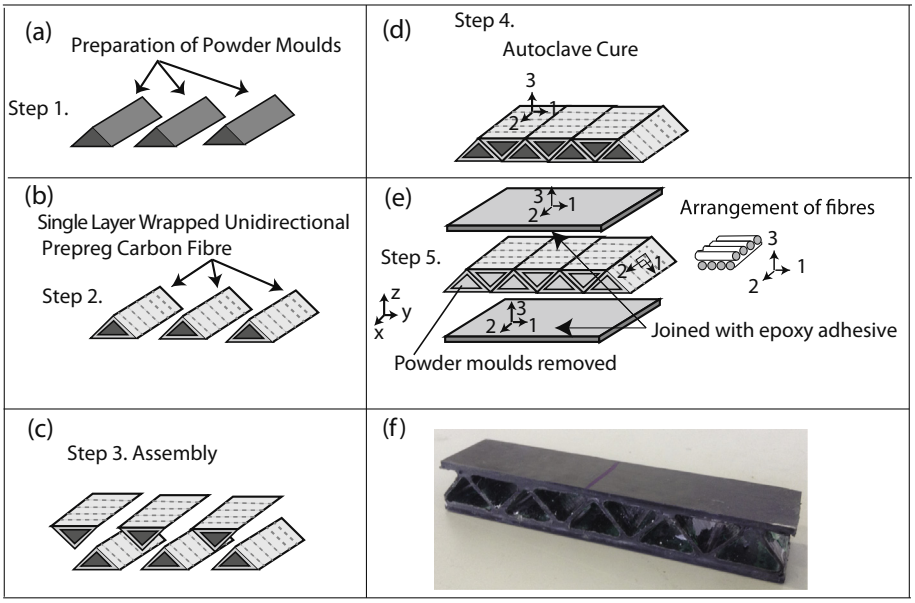

Fig. 1. The 5–step process to manufacture the composite sandwich structure with corrugated core [(a) – (e)] and an example sandwich beam after completion (f). The local coordinate system 1-2-3 is shown in the figure with axis-1 aligned with fibre direction on surface layers.

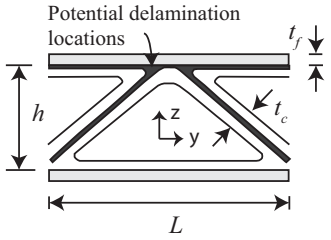

Fig. 2. Geometry of the unit cell within the sandwich core with $L = 30$ mm, $h = 15$ mm, $t_f = 2.8$ mm and $t_c = 1.4$ mm. Locations of potential delamination are highlighted in black.

0/90° and ±45° with respect to the loading direction. The results are presented in Fig. 3(a). For fibres orientated along 0/90° direction, samples failed with a brittle fibre fracture of properties dominated longitudinal fibres. The material response tested with fibres orientated along the ±45° direction was dominated by the matrix. The final failure was of shear failure of the matrix resulting in fibre pullout.

3.2. Quai-static compressive testing on the base material

Quasi-static compressive tests were conducted on rectangular specimens of gauge length $l_1 = 10$ mm, width of $b_1 = 25$ mm and thickness $\delta_1 = 6.35$ mm. No global buckling was observed during the quasi-static compressive testing. The ply layup for the specimens has a total of 8 plies of orientation $[90/0/90/0]_{sym}$ with 0° orientated along the loading direction. Specimens were tested at three different loading rates, i.e. 1, 25 and 50 mm per minute. The test results are shown in Fig. 3(b). At these loading rates, there was no significant difference in the stiffness of the specimen, and only a marginal increase in the strength. The final failure was of brittle fracture of longitudinal fibres accompanied by inter and intra-lamina matrix cracking leading a mushrooming of the specimen. The failure of the UD-laminate materials under compressive loading has been extensively investigated and attributed to plastic micro-buckling of fibres [18,19]. Five specimens were tested in both tension and compression coupon tests.

3.3. Quasi-static compressive testing of composite cores

An Instron 5581 screw driven testing machine provided a constant quasi-static displacement in the through-thickness direction (z-direction in Fig. 2). The samples consisting of a single core unit cell, of base length $L = 30$ mm, width along x-axis $w = 27.5$ mm and height $h = 15$ mm (Fig. 2), were cut from the cured composite sandwich plates. Samples were tested at a constant cross-head speed of 2 mm/min. Load F and vertical deflection δ of the crosshead were both measured directly from the Instron test machine. The nominal core compressive stress is defined as $\sigma_c = F/Lw$, and the nominal core compressive strain is defined as $\varepsilon_c = \delta/h$. Two representative results of the quasi-static core crush test are presented in Fig. 4(a). Quasi-static compression tests were also performed on the composite core samples consisting of two core unit cells, giving a total length of 60 mm, in order to confirm the validity of the assumption that the response of one unit cell was representative of the corrugated cores. Tests were performed at 3 different loading rates; 1, 10 and 50 mm per minute. The results for the double unit cell core experiments are presented in Fig. 4(b). It was demonstrated that the stress-strain response of the double unit cell cores were the same to that of the singular unit cell cores, including failure mechanism. It was also noted that there was no significant difference in the response of the cores throughout the loading rates tested.

As observed in the test (also shown in Fig. 10 in Section 4), the peak nominal stresses experienced during the quasi-static experiments correspond to the onset of damage of the base composite material at the bottom joints of the core webs. This is due to the fact that the tests were conducted on the unconstrained cores and the core webs were free to expand laterally during the test. These joints prove to be a weak point for the core design, whose strength is dominated by the shear strength of the base composite material. Examination of the nature of damage and position of the fracture surface is presented in Fig. 5, with (a) showing the fracture surface of a single unit cell core and (b) showing the fracture surface of a double unit cell core. The quasi-static test results confirmed that the response of one unit cell was representative of the corrugated cores under compression.

3.4. Dynamic compression test protocol

The dynamic compressive responses of the base material and the wrapped sandwich core were measured using a series of direct impact tests via strain-gauged Kolsky bar test system [20]. The dynamic test set-up is presented in Fig. 6(a) and (b) for the wrapped composite cores and UD-laminate base material, respectively. For the core testing, one representative unit cell of the sandwich panel was tested. As demonstrated in the quasi-static compressive test, the response of one unit cell was representative of the corrugated cores. For the base composite material tests, the material coupons identical to the ones within the quasi-static compressive test was used, with 1-direction as the loading and fibre direction. The specimens were placed centrally on the front end of the Kolsky bar and a steel striker of the same material properties to the Kolsky bar was fired by a gas gun to impact the specimens. Strain gauges located at the centre of the Kolsky bar was used to record the stress in the distal face of the specimens from impact.

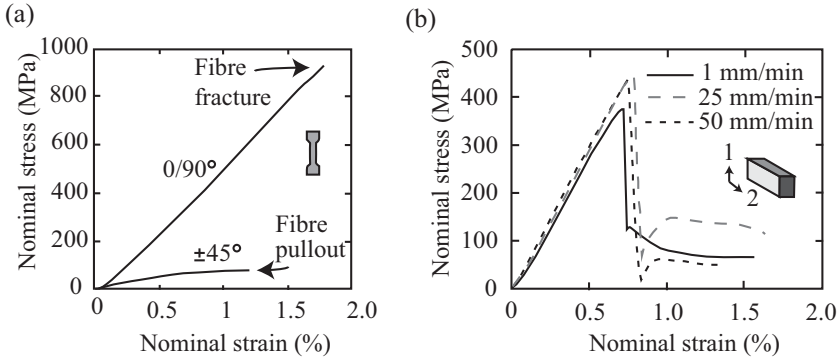

Fig. 3. Quasi-static uniaxial testing for the composite base material: (a) dogbone tensile test, and (b) compressive coupon test.

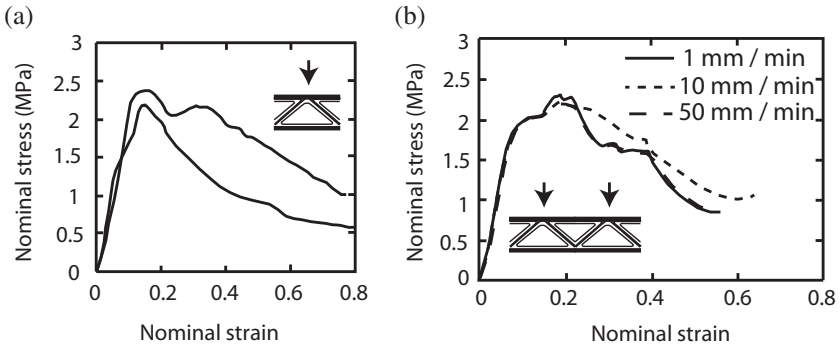

Fig. 4. Quasi-static compressive test of the sandwich core: (a) single unit cell test, and (b) double unit cell test at selected loading rates.

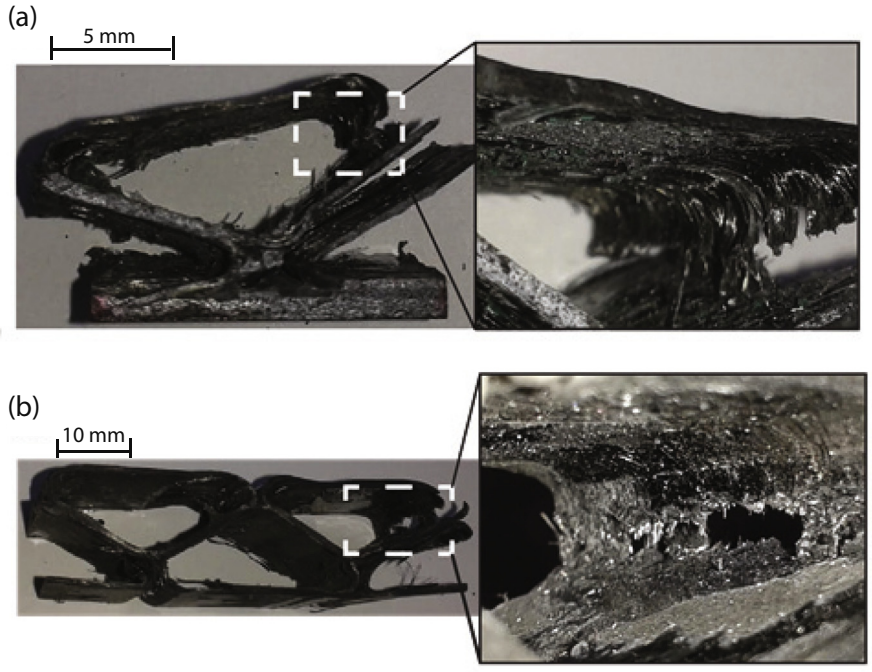

Fig. 5. Damage mode of wrapped composite cores during quasi-static compressive testing: (a) single unit cell, and (b) double unit cell.

To ensure a constant strain rate throughout each test, the striker was required not to significantly decelerate as it impacts the sample. Striker masses were tailored to suit this need. In the lower velocity range (up to $v_0 = 25\ \mathrm{ms}^{-1}$), a larger striker of length 0.5 m and mass M = 2.4 kg was used; for velocity range higher than $v_0 = 25\ \mathrm{ms}^{-1}$, a smaller striker of length 0.1 m and mass M = 0.475 kg was used. The high-speed photography using a Phantom V12 camera confirmed that the deceleration of strikers was negligible during the dynamic compressive tests.

The striker was accelerated using a pressurised gas gun of barrel length 3.5 m and internal diameter of 28 mm. The strikers each had a diameter of 27.5 mm so a sabot was not required for firing. At lower velocities, and thus lower pressures, $P \leqslant 6.5$ bar, compressed air was used to pressurise a 3-litre diving cylinder in order to drive the strikers. At higher velocities / pressures ($P \geqslant 6.5$ bar), pressurised nitrogen (oxygen-free) was utilised. The range of the striker velocity was $2.5 \leqslant v_0 \leqslant 120\ \mathrm{ms}^{-1}$. The striker velocity was measured using two laser gates located at the open end of the gas gun barrel and confirmed with the high speed camera measurement. The Kolsky bar was positioned 110 mm from the open end of the gas gun. The Kolsky bar had a diameter identical to that of the strikers of 27.5 mm, a length of 1.8 m and was of standard set-up. Both the Kolsky bar and the strikers were made from M300 maraging steel with yield strength of 1900 MPa. The Kolsky bar was supported by four knife-edge friction-reducing Nylatron bearings and momentum was resisted at the distal end by an ACE MA 4757M self-adjusting shock absorber. Two diametrically opposite 120 Ω TML foil strain gauges of gauge length 1 mm in a half-Wheatstone bridge were located at the centre point. The stress history was recorded as a voltage change from the strain gauges, which was amplified by a Vishay 2310B signal conditioning amplifier system before being recorded on an Instek GDS-1052-U 50 MHz 2-channel Digital Oscilloscope. During capturing of the signals, the two diametrically opposite strain gauges allowed for a simple check for any bending in the Kolsky Bar. Any bending will produce sinusoidal oscillations with a π phase-difference between the two channels. If negligible bending was recorded during the test, the results were accepted and the average value of the two gauges was taken.

A calibration test was conducted by impacting the large striker against the Kolsky bar at a velocity $v_0 = 4.1\ \mathrm{ms}^{-1}$. The stress history measured by the Kolsky bar is plotted in Fig. 7. Also presented

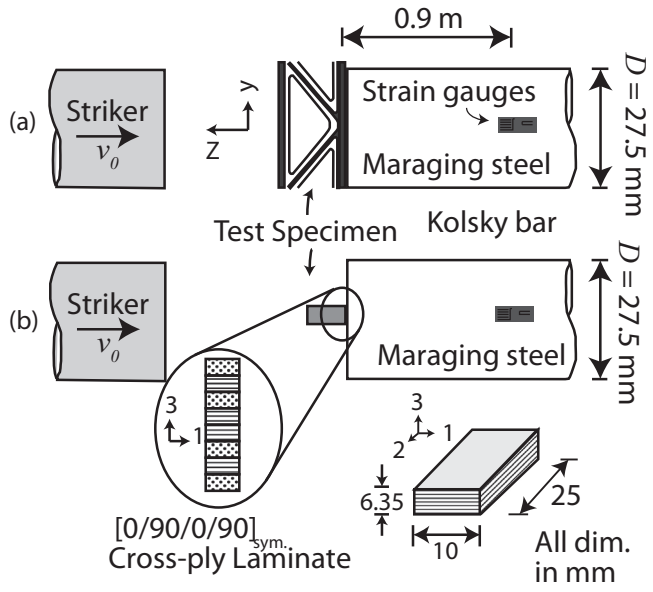

Fig. 6. Sketch of dynamic compressive tests for (a) a wrapped carbon fibre composite core with single unit cell and (b) a UD laminate.

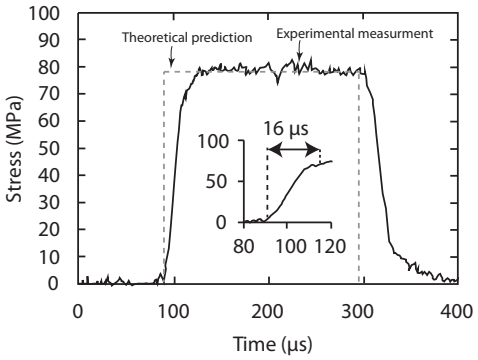

Fig. 7. The time history of the dynamic stress measured via Kolsky bar with striker of length L = 0.5 m and diameter D = 27.5 mm impacting upon a Kolsky pressure bar with the same diameter at velocity v_0 = 4.1 m/s. Also shown is the theoretically predicted stress pulse calculated from 1D elastic wave theory and the onset of the stress pulse in the insert.

in the figure is the predicted stress using 1D elastic wave theory, which states that the axial stress within the bar during the event is $\sigma_E = \rho_s c v_0/2 = 77.1$ MPa with ρ_s and c as the maraging steel density and longitudinal elastic wave speed, respectively. The average measured stress throughout the calibration test was 78.5 MPa, within 2% of the prediction. The longitudinal elastic wave speed was measured experimentally as the time taken for the reflection of the compressive wave from the distal end of the Kolsky bar returning to the strain gauges as a tensile wave. It was measured as 4865 ms^{-1}, giving a time taken for reflection and thus complication of the stress measurement as 370 μs. As shown in the insert of the figure, the measured pulse took approximately 16 μs to reach the predicted stress level, which represents the response time of the whole measurement system. The response time of the whole measurement system is mainly governed by the response time of strain gauges employed in the testing. Experiments have confirmed that the response time of the measurement system is independent of the velocity of the striker. This sets the limit of the system in measurement of the dynamic response. This limit is negligible for low speed impact events, but may have significant influence for high velocity impact events, i.e. the significant compression of the specimen is achieved within the time scale less than the response time of the measurement system. In the next section, we will demonstrate, even though the limit prevents accurate measurement of the dynamic stiffness of specimens, the peak stresses could be accurately captured by the measurement system.

4. Experimental results of dynamic compression tests

4.1. Base material test results

For thorough analysis of the dynamic compressive response of the wrapped composite cores, it was necessary to determine the strain-rate sensitivity of the base UD-laminate material. Material coupons were impacted by the strikers at the velocities ranging from $11\ ms^{-1} \leqslant v_0 \leqslant 92\ ms^{-1}$, giving a nominal strain rate $\dot{\varepsilon} \equiv v_0/l_1$ from 1100 s^{-1} to 9200 s^{-1}. The nominal stress measured at the distal side of the sample (the opposite side of the sample to the striker impact) is plotted against the normalised time $\bar{t} \equiv v_0 t/h$ with t as the time after impact in Fig. 8(a) for selected samples. The stress within the sample is calculated from the stress measured within the bar by a ratio of surface areas of sample to bar. It should be noted that, as the system response time of the set-up is approximately 16 μs, see Section 3.4, it is not possible to take accurate measurements of the dynamic stiffness of the composite material as elastic response occurs within the system response time. However, the measurement of the peak stresses throughout the tests is accurate and reflects the material property. This can be explained by considering the maximum impact velocity employed in the test, i.e. $v_o = 92\ ms^{-1}$. The time to achieve peak stress is t_o = 16.3 μs that is approximately identical to the system response time. In addition, as the elastic wave speed of the base carbon fibre composite material is approximately c = 5000 m/s, the elastic wave

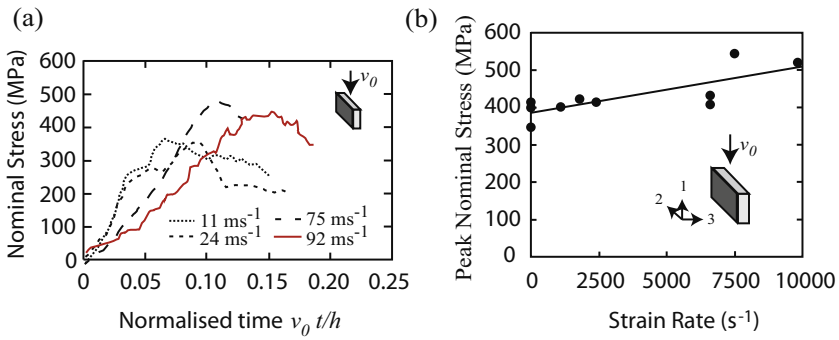

Fig. 8. Dynamic compressive testing of base composite material (a) nominal stress versus normalised time for selected samples under different velocities, and (b) peak nominal stress versus strain rate.

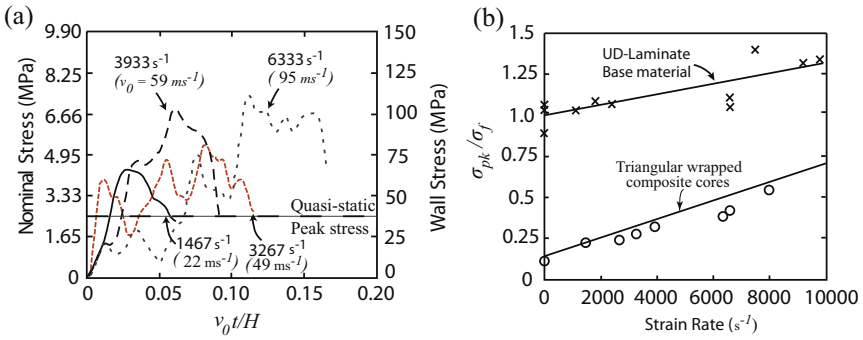

Fig. 9. (a) Nominal core compressive stress or strut wall stress as a function of normalised time for wrapped composite cores across a range of strain-rates, and (b) peak strut wall stress normalised by quasi-static compressive strength of the base material as a function of applied strain rates for the wrapped composite cores. Also presented in (b) is the normalised peak stress of the UD-laminate base material as a function of applied strain rates.

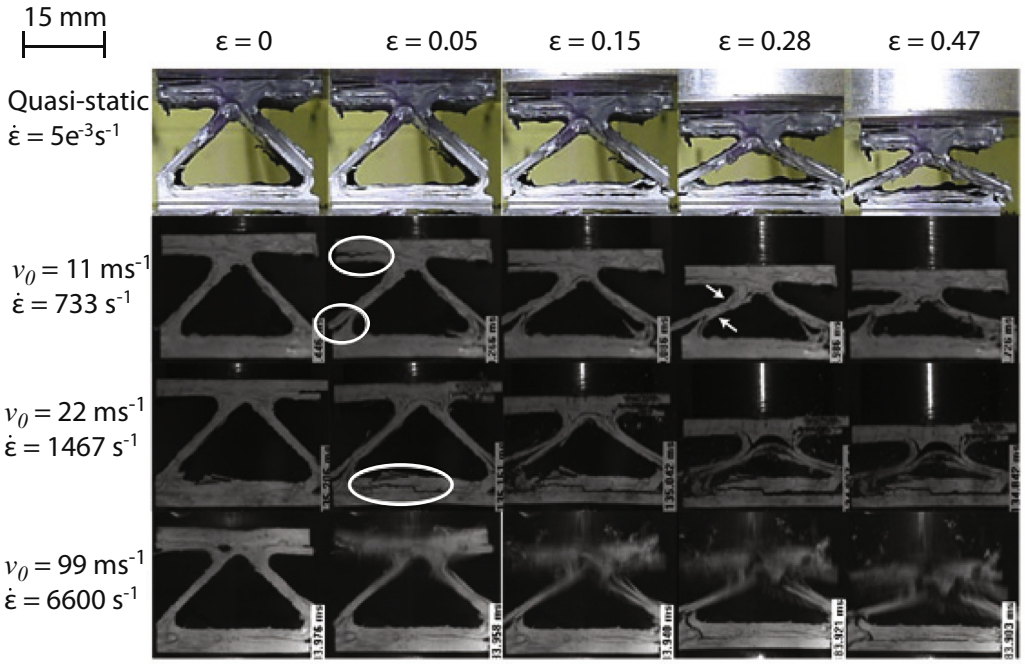

Fig. 10. Montage of dynamic crush event for four different applied strain rates, demonstrating different damage mechanisms (i) $\dot{\varepsilon} = 5 \times 10^{-3}$ s^{-1} progressive unwrapping (ii) $\dot{\varepsilon} = 733$ s^{-1} delamination-buckling of struts (iii) $\dot{\varepsilon} = 1467$ s^{-1} combination of delamination-buckling of struts and compressive fibre fracture of struts and (iv) $\dot{\varepsilon} = 6600$ s^{-1} crushing of composite material in the struts. Regions of delamination within the cores are highlighted.

takes $t = 2$ μs to reach the distal side of the specimen. Hence, at least 8 elastic wave reflections had taken place in the specimen when the peak stress was achieved: the specimen was under axial equilibrium for the measurement of the peak stress. Hence, we conclude the peak stresses measured in the experiment reflect material property.

As shown in Fig. 8(a), as the striker was under a constant velocity, the peak stresses for the material coupons occurred at higher strain than that obtained by quasi-static compressive test (Fig. 3 (b)). However, the failure mode during the high strain rate tests is identical to that of the quasi-static test, i.e. a brittle fracture of longitudinal fibres with inter and intra-laminar matrix cracking. This is the typical failure mode for high strain rate compressive testing of UD-laminate carbon/epoxy [21]. Dependency of the peak stress of the parent material upon the imposed strain rate $\dot{\varepsilon}$ is shown in Fig. 8(b). The peak stress increases by about 105 MPa within the strain rate range of 10^{-3} s^{-1} to 10^{4} s^{-1}. For simplicity, the trend could be approximated as a linear function. The linear increase in peak stress exhibited during the test is attributed to the strain-rate dependency of the matrix delaying the onset of fibre microbuckling. This could be demonstrated by the phenomenon that peak stresses for material coupons occur at higher strain for higher velocity impact, as shown in Fig. 8(a). The outcome of the dynamic compressive tests for wrapped composite cores will be discussed next.

4.2. High strain rate testing for wrapped composite cores

The dynamic compressive response of the wrapped composite corrugated cores is shown in Fig. 9(a) for time history of nominal core compressive stress, σ_c, and the strut wall stress, σ_s, respectively, for selected compressive strain rates. Here, the strain rate for core compression is defined as $\dot{\varepsilon} \equiv v_0/h$. The two stresses could be related through the following equation

$$\sigma_c = 2\left(\frac{t_c}{\sqrt{h^2 + L^2/4}}\right)\left(\frac{h}{L}\right)\sigma_s \quad (1)$$

The peak stresses of the composite corrugated cores were achieved at time scale more than system response time, i.e. t = 16–19 μs. As mentioned in Section 3.4, with this time scale, the accurate measurement of the peak stresses throughout the tests can be achieved. However, the measurement of the dynamic stiffness is not accurate. The peak wall stress, normalised by the quasi-static compressive strength of the base material, is shown in Fig. 9(b) as a function of strain rate. The experimental data can be approximately fitted with a linear relationship. The functional relationship between dynamic compressive strength of the base material and strain rate is also shown in the figure for comparison. The wrapped composite cores exhibited higher strain rate sensitivity to that of the base composite material. With increasing strain rate, up to approximately 8200 s^{-1}, the peak compressive stress increases around 2.8 times. We will later show the dominant factor for strength enhancements of the wrapped composite cores under different strain rates is microinertial effects rather than material rate sensitivity.

To examine the failure mechanisms of the composite cores under compressive loading of different strain rates, the montages of the high speed photographs showing the deformation of the wrapped composite core undergoing compressive loading for $\dot{\varepsilon} = 5 \times 10^{-3}, 733, 1467$ and 6600 s^{-1} are presented in Fig. 10. The four representative strain rates show distinctly different deformation mechanisms. The quasi-static response, shown in Fig. 10 for strain rate $\dot{\varepsilon} = 5 \times 10^{-3}$ s^{-1}, exhibited a failure mode of progressive "unwrapping" of the cores due to matrix fracture at the join locations. At tests within the strain rate range 350 $s^{-1} \leqslant \dot{\varepsilon} \leqslant$ 750 s^{-1}, the unwrapping mechanism was suppressed, due to microinertial effects, to allow for the failure mechanism to become that of delamination-buckling of the struts. Delamination was first observed within the struts closed to distal end. The predicted location of delamination is highlighted in Fig. 2 and the experimentally observed location of delamination is circled in Fig. 10 for strain rate $\dot{\varepsilon} = 733$ s^{-1}. Delamination will cause the effective thickness of the struts to decrease, allowing for bucking to occur. This failure mode is seen to gradually overlap with the third failure mechanism. The failure mechanism exhibited approximate strain rate range 1000 $s^{-1} \leqslant \dot{\varepsilon} \leqslant$ 4000 s^{-1} is a combination of delamination-buckling and fracture of material within the struts. This is demonstrated with the third montage in Fig. 10 for $\dot{\varepsilon} = 1467$ s^{-1}.. At the highest strain rates $\dot{\varepsilon} \geqslant$ 4000 s^{-1}, the buckling of the struts was suppressed by microinertial effects. The failure mechanism is dynamic crushing in the material of the struts. This is demonstrated in the montage in Fig. 10 for $\dot{\varepsilon} = 6600$ s^{-1}. The failure mechanisms at different strain rate ranges demonstrate that the strength enhancements of the wrapped composite cores under different strain rates are mainly induced by microinertial effects.

5. Concluding remarks

A novel method of sandwich panel manufacturing was developed utilising tessellating wrapped cores of pre-impregnated carbon fibre reinforced epoxy composites. Pre-impregnated laminate tapes were wrapped around destructible triangular prism cores. These wrapped cores were tessellated top to bottom to create a full sandwich panel core. Standard vacuum bagging technique was utilised for composite curing, and carbon fibre reinforced epoxy 0/90 UD-laminate face sheets were attached with epoxy adhesive.

The base composite material was tested in compression over a range of strain rates 1.66×10^{-1} $s^{-1} \leqslant \dot{\varepsilon} \leqslant$ 9200 s^{-1} using an instrumented screw-driven testing rig for quasi-static and a direct impact Kolsky bar test system for high strain-rate tests, respectively. The base material was found to exhibit certain rate-dependency behaviour. Material rate dependency was attributed to compressive micro-buckling stabilisation of longitudinal fibres. Wrapped composite cores of relative density $\bar{\rho} = 0.13$ were tested in quasi-static and dynamic compressive experiments. Cores were provided with no lateral confinement and quasi-static failure was that of progressive unwrapping of cores due to matrix cracking at the joints of the core webs. Wrapped carbon fibre composite cores demonstrated rate-dependent behaviour for strain rate range tested. This was attributed to the suppression of the failure mode demonstrated during quasi-static testing, and inertial stabilisation of struts against buckling leading to an upper-bound failure mechanism of crushing of carbon fibre material within the struts.

Acknowledgements

The authors acknowledge support from the Engineering and Physical Sciences Research Council, UK (EPSRC EP/P505658/1 and EP/K503101/1) and Early Career Research and Knowledge Transfer Awards from the University of Nottingham.

References

[1] Liu T, Deng ZC, Lu TJ. Design optimization of truss-cored sandwiches with homogenization. Int J Solids Struct 2006;43:7891–918.
[2] Liu T, Fleck NA, Wadley HNG, Deshpande VS. The impact of sand slugs against beams and plates: coupled discrete particle/finite element simulations. J Mech Phys Solids 2013;61(8):1798–821.
[3] Dharmasena KP, Wadley HN, Liu T, Deshpande VS. The dynamic response of edge clamped plates loaded by spherically expanding sand shells. Int J Impact Eng 2013;62:182–95.
[4] Fleck N, Deshpande V. The resistance of clamped sandwich beams to shock loading. J Appl Mech 2004;71:386–401.
[5] Ashby M, Evans A, Fleck N, Gibson L, Hutchinson J, Wadley H, Delale F. Metal foams: a design guide. Appl Mech Rev 2001;54:105.
[6] Wadley HN. Cellular metals manufacturing. Adv Eng Mater 2002;4:726–33.
[7] Sugimura Y, Meyer J, He M, Bart-Smith H, Grenstedt J, Evans A. On the mechanical performance of closed cell Al alloy foams. Acta Mater 1997;45:5245–59.
[8] Chen C, Harte A, Fleck N. The plastic collapse of sandwich beams with a metallic foam core. Int J Mech Sci 2001;43:1483–506.
[9] Deshpande V, Fleck N. Isotropic constitutive models for metallic foams. J Mech Phys Solids 2000;48:1253–83.
[10] Wadley HN, Fleck NA, Evans AG. Fabrication and structural performance of periodic cellular metal sandwich structures. Compos Sci Technol 2003;63:2331–43.
[11] Liu T, Deng ZC, Lu TJ. Minimum weights of pressurized hollow sandwich cylinders with ultralight cellular cores. Int J Solids Struct 2007;44(10):3231–66.
[12] Deshpande V, Fleck N. Collapse of truss core sandwich beams in 3-point bending. Int J Solids Struct 2001;38:6275–305.
[13] Xue Z, Hutchinson JW. A comparative study of impulse-resistant metal sandwich plates. Int J Impact Eng 2004;30:1283–305.
[14] Liu T, Deng ZC, Lu TJ. Bi-functional optimization of actively cooled, pressurized hollow sandwich cylinders with prismatic cores. J Mech Phys Solids 2007;55(12):2565–602.
[15] Russell B, Malcom A, Wadley H, Deshpande V. Dynamic compressive response of composite corrugated cores. J Mech Mater Struct 2010;5:477–93.
[16] Russell B, Deshpande V, Wadley H. Quasistatic deformation and failure modes of composite square honeycombs. J Mech Mater Struct 2008;3:1315–40.
[17] Turner P, Liu T, Zeng X. Dynamic response of orthogonal three-dimensional woven carbon composite beams under soft impact. J Appl Mech 2015;82(12):121008.
[18] Jelf F, Fleck N. Compression failure mechanisms in unidirectional composites. J Compos Mater 1992;26:2706–26.
[19] Hahn HT, Williams JG. Compression failure mechanisms in unidirectional composites. Compos Mater: Testing Des 1986:115–39.
[20] Kolsky H. An investigation of the mechanical properties of materials at very high rates of loading. Proc Phys Soc London, Sect B 1949;62:676.
[21] Hosur M, Alexander J, Vaidya U, Jeelani S. High strain rate compression response of carbon/epoxy laminate composites. Compos Struct 2001;52:405–17.